sustainability

MDPI

Article

Seasonal Variations of $PM_{2.5}$ Pollution in the Chengdu–Chongqing Urban Agglomeration, China

Kun Wang [1,2], Yuan Yao [1,2,3,*] and Kun Mao [1,2]

[1] School of Architecture and Civil Engineering, Chengdu University, Chengdu 610106, China; wangkunchengdu@aliyun.com (K.W.); mk15881975667@aliyun.com (K.M.)
[2] Key Laboratory of Pattern Recognition and Intelligent Information Processing of Sichuan Province, Chengdu University, Chengdu 610106, China
[3] State Key Laboratory of Resources and Environment Information System, Institute of Geographical Sciences and Natural Resources Research, Chinese Academy of Sciences, Beijing 100101, China
* Correspondence: yaoyuan@cdu.edu.cn; Tel.: +86-028-84616416

Abstract: During the development of the Chengdu–Chongqing Urban Agglomeration (CCUA) in China, $PM_{2.5}$ pollution severely threatened public health, presenting a significant environmental challenge. This study employs a novel spatial interpolation method known as High Accuracy Surface Modeling (HASM), along with the geographical detector method, local and regional contributions calculation model, and the Hybrid Single–Particle Lagrangian Integrated Trajectory model to analyze the seasonal spatial distribution of $PM_{2.5}$ concentrations and their anthropogenic driving factors from 2014 to 2023. The transport pathway and potential sources of seasonal $PM_{2.5}$ concentrations were also examined. The results showed the following: (1) HASM was identified as the most suitable interpolation method for monitoring $PM_{2.5}$ concentrations in the CCUA; (2) The $PM_{2.5}$ concentrations exhibited a decreasing trend across all seasons, with the highest values in winter and the lowest in summer. Spatially, the concentrations showed a pattern of being higher in the southwest and lower in the southeast; (3) Industrial soot (dust) emissions (ISEs) and industry structure (IS) were the most important anthropogenic driving factors influencing $PM_{2.5}$ pollution; (4) The border area between the eastern part of the Tibet Autonomous Region and western Sichuan province in China significantly contribute to $PM_{2.5}$ pollution in the CCUA, especially during winter.

Keywords: $PM_{2.5}$; HASM; seasonal variation; driving factors; potential source contribution

check for updates

Citation: Wang, K.; Yao, Y.; Mao, K. Seasonal Variations of $PM_{2.5}$ Pollution in the Chengdu–Chongqing Urban Agglomeration, China. *Sustainability* **2024**, *16*, 9242. https://doi.org/10.3390/su16219242

Academic Editor: Anmin Duan

Received: 23 August 2024
Revised: 18 October 2024
Accepted: 23 October 2024
Published: 24 October 2024

Copyright: © 2024 by the authors. Licensee MDPI, Basel, Switzerland. This article is an open access article distributed under the terms and conditions of the Creative Commons Attribution (CC BY) license (https://creativecommons.org/licenses/by/4.0/).

1. Introduction

In recent years, China's rapid economic growth and urban expansion have led to a significant increase in atmospheric emissions and air pollution [1]. Air pollution originates from various sources, both human–made and natural, such as the burning of fossil fuels for agriculture, transportation, household use, industrial activities, electricity, and waste processing [2,3]. Several studies investigated $PM_{2.5}$ pollution in the North China Plain, with particular interest in the Hebei province, as well as in the Tianjin–Beijing metropolitan area and its surrounding areas [4–6]. The studies focus on the Chengdu–Chongqing Urban Agglomeration (CCUA) located in the complex terrain of the Sichuan Basin. Despite the increasing population migration from other cities to the CCUA, research on this area remains limited. The CCUA's population has increased by nearly 1 million on average annually over the past three years, with the total reaching 98.7 million in 2023. With the rapid urbanization process, the CCUA has experienced more frequent poor air quality days, higher emissions of air pollutants, and increased energy consumption during the past 30 years [7]. Anthropogenic factors, such as population growth, economic activities, and energy consumption, are essential socioeconomic determinants of $PM_{2.5}$ pollution [8]. Understanding the spatial variation of $PM_{2.5}$ across different seasons, along with the

associated anthropogenic driving factors in urban agglomerations, is crucial for developing effective and efficient air pollution control measures.

However, air quality monitoring stations within regional regulatory networks are relatively sparse due to the high cost of construction. Consequently, the data from these stations do not fully capture the real–time spatial distribution of air pollution in the region [9]. Currently, satellite remote sensing data collected from space–based sensors are commonly applied to generate spatial distributions of air pollutant concentrations [10,11]. However, satellite data are easily affected by cloud cover, which can lower the performance and accuracy of satellite images. Additionally, satellite data for a given region are not continuous, with intervals between available images ranging from hours to years. As a result, remote sensing may offer limited and inaccurate representations of air pollution distribution. Given the limitations of satellite image–based approaches, spatial interpolation and extrapolation technologies are employed to estimate values for non–monitored stations using data from measured or known monitoring sites within the area [12,13]. Point–based interpolation/extrapolation such as universal Kriging (UK), original Kriging (OK), spline interpolation and Inverse Distance Weighting (IDW) are the most frequently used methods. For example, Halimi et al. found OK was the best method to estimate PM_{10}, NO_2, and CO concentrations in Tehran as compared to different Kriging interpolation methods during 2012 and 2014 [14]. Yu et al. applied 14 methods to estimate the eight pollutants in Atlanta and found that IDW and Kriging were better suited for estimating secondary pollutants [15]. However, the performance of traditional interpolation methods in characterizing highly variable near–surface or atmospheric conditions has long been troubled by errors, and no optimum method has proven to be consistently superior to others [16–18]. These methods use only the information from sample sites within a local neighborhood. These methods can produce steep gradients if the spatial sampling points are too sparse, leading to potential inaccuracies. For instance, Goovaerts et al. noted that Kriging depends heavily on a well–chosen semivariogram, which can be challenging to estimate and validate against the true covariance function [19]. Magnussen et al. pointed out that IDW overlooks the spatial structure and information beyond the local neighborhood of the sample points [20]. Similarly, Wang et al. observed that spline interpolation uses univariate cubic basis splines to approximate surfaces, but this approach often fails to accurately represent surfaces due to limitations in univariate cubic spline formulations [21].

To overcome the limitations, the High Accuracy Surface Modeling (HASM) method was proposed as an effective alternative [22]. This method applies the fundamental theorem of surfaces to approximate the surface using a least squares approach, resulting in a highly accurate model for spatial interpolation [23]. Its precision has made it a practical choice for applications such as digital soil mapping [24], DEM construction [25], and precipitation estimating [26] due to its high accuracy.

Thus, the main objectives of this study are to accomplish the following: (1) estimate the spatial distribution of $PM_{2.5}$ concentrations across different seasons in the CCUA from 2014 to 2023 using HASM; (2) clarify the relationship between seasonal $PM_{2.5}$ concentrations and their anthropogenic factors; and (3) analyze the transport pathways and potential source region contributions of $PM_{2.5}$ in four seasons.

2. Data and Methods

2.1. Study Area

The CCUA, located between 101°56′33″–110°12′21″ E and 27°39′43″–33°02′10″ N, encompasses 15 cities in the Sichuan province and Chongqing city, covering an area of 185,000 square kilometers. According to the 2023 census data, the CCUA supports a population of 97.70 million residents and has a gross domestic product (GDP) of USD 1.10 trillion. The CCUA is primarily located within the Sichuan Basin, which is characterized by a complex topography with a pronounced gradient of higher elevations in the west and lower elevations in the east (Figure 1). The central region of the CCUA features relatively flat terrain, predominantly consisting of alluvial plains, while the periphery exhibits varied

topography, including the Longmen Mountains to the northwest, the Qionglai Mountains to the southwest, the Wuling Mountains to the southeast, and the Daba Mountains to the northeast. The region experiences a subtropical monsoon climate, with an annual average temperature ranging from 16.4 °C to 18 °C and annual precipitation between 1107.8 mm and 1406.4 mm.

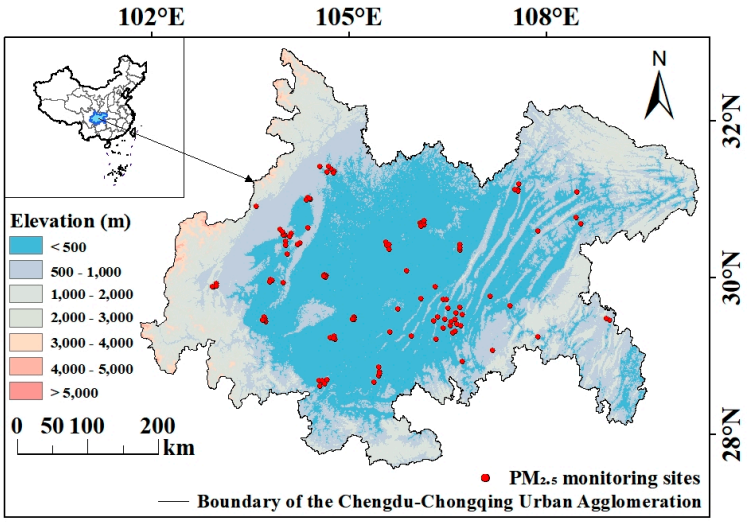


Figure 1. $PM_{2.5}$ monitoring sites in the Chengdu–Chongqing Urban Agglomeration.

2.2. Data Source and Description

Monthly $PM_{2.5}$ concentration data from 134 monitoring stations within the CCUA are collected from the China National Environmental Monitoring Center, spanning from March 2014 to February 2024. The data are categorized into four seasons: spring (March to May), summer (June to August), autumn (September to November), and winter (December to February). Previous studies showed that anthropogenic factors, including household activities, economic activities, and industrial structures, are key determinants of $PM_{2.5}$ concentrations. In this study, seven anthropogenic driving factors (Table 1), such as gross domestic product (GDP), foreign direct investment (FDI), industry structure (IS), industrial soot (dust) emissions (ISE), population density (PD), electricity consumption (EC), and road density (RD), were selected for analyzing seasonal $PM_{2.5}$ pollution in the CCUA. The global data assimilation system (GDAS) is used to simulate meteorological fields and provide numerical weather predictions. Although the GDAS dataset is widely used in meteorological and environmental research, it relies on global observation stations. However, in certain regions with a low density of observation stations, it may result in less accurate meteorological information for those areas [27].

Table 1. Summary of data used in this study.

Data Type	Data Name	Spatial Resolution	Temporal Frequency	Time	Data Source
Air quality data	$PM_{2.5}$ [1]	/	monthly	2014–2024	http://www.cnemc.cn/ (accessed on 1 June 2024)
Anthropogenic data	GDP [2]	/	monthly	2014–2023	Sichuan Provincial Bureau of Statistics Chongqing Statistical Bureau
	FDI [3]	/			
	IS [4]	/			
	ISE [5]	/			
	EC [6]	/			
	PD [7]	/	yearly		https://www.stats.gov.cn/ (accessed on 1 July 2024)
	RD [8]	/			https://jtt.sc.gov.cn/ (accessed on 1 July 2024)

Table 1. *Cont.*

Data Type	Data Name	Spatial Resolution	Temporal Frequency	Time	Data Source
Meteorological data	GDAS [9]	1°	hourly	2014–2024	https://www.noaa.gov/ (accessed on 1 July 2024)
	RH [10]	1 km	monthly	2014–2020	https://data.tpdc.ac.cn/ (accessed on 1 July 2024)
	TEM [11]	1 km			
	PRE [12]	1 km		2014–2021	
	WS [13]	1 km			

[1] $PM_{2.5}$ concentration; [2] gross domestic product; [3] foreign direct investment; [4] industry structure; [5] industrial soot (dust) emissions; [6] electricity consumption; [7] population density; [8] road density; [9] global data assimilation system; [10] relative humidity; [11] air temperature; [12] precipitation; [13] wind speed.

2.3. Methodology

2.3.1. HASM

Currently, HASM, developed by Yue et al. [22], has been extensively applied in spatial interpolation such as DEM [28], CO_2 [29], air temperature [30], and precipitation [31]. Studies by Zhao et al. [26] and Liu et al. [29] demonstrated that HASM effectively addresses errors and multiscale issues, providing improved accuracy in predicting variables.

Regarding the fundamental surface theorem, if a surface can be expressed as $X = f(x,y)$, the HASM expression is as follows:

$$\begin{cases} \min \left\| \begin{bmatrix} A_1 \\ A_2 \\ A_3 \end{bmatrix} \cdot X^{(n+1)} - \begin{bmatrix} a^{(n)} \\ b^{(n)} \\ c^{(n)} \end{bmatrix} \right\| \\ \text{s.t.} S \cdot X^{(n+1)} = k \end{cases} \quad (1)$$

where $X^{(n+1)}$ represents the $(n+1)$-th iteration of the estimated points within the study area. The coefficient matrices corresponding to the first, second, and third equations of HASM are denoted as A_1, A_2, and A_3, respectively. The vectors $a^{(n)}$, $b^{(n)}$, and $c^{(n)}$ represent the right–hand sides of the HASM master equation, k denotes the sampling number, and S represents the sampling matrix.

In this study, $PM_{2.5}$ concentration data from 134 stations in the CCUA were divided into an interpolating dataset and validating dataset: 70% of the data were used to interpolate, while the remaining 30% were employed for validate. Additionally, the performance of HASM was evaluated by root mean square error (RMSE) and the coefficient of determination (R^2) based on the validating dataset [32]. A smaller RMSE value and larger R^2 value indicate greater prediction accuracy.

2.3.2. HYSPLIT Backward–Trajectory Models

As a widely used method to generate air mass backward trajectory hybrid diffusion models [33–35], the HYSPLIT model was employed to investigate the backward trajectory and diffusion of $PM_{2.5}$ pollutants in the CCUA. In this study, meteorological data with a resolution of 1° latitude × 1° longitude and hourly intervals (00:00–23:00 UTC) from the GDAS were used to calculate 48 h backward trajectories at 500 m above ground level from March 2014 to February 2024, incorporating seasonal calculations.

2.3.3. Local and Regional Contribution Calculation Model

Many scholars worldwide have found that $PM_{2.5}$ concentrations are influenced not only by local emissions but also significantly by regional transport, which is attributed to both local and regional sources. Therefore, estimating the contributions of regional pollutant transport is crucial for accurately assessing the impact of local emission sources. Thus, separately estimating the contributions of local emissions and regional pollutant transport is crucial for accurately assessing the impact of local emission sources.

In this study, the local and regional contribution calculation model [36] proposed by Lv et al. was used to estimate the local and regional contribution of seasonal $PM_{2.5}$ concentrations in the CCUA from 2014 to 2023. The model can be expressed as follows:

$$Local\ contribution(LP) = \frac{\sum(N_i \times C_i)}{\sum N_i \times C_{avg}} \quad (2)$$

$$Regional\ contribution(P_i) = \frac{N_i \times (C_i - C_{min})}{\sum_{i=1}^{m}[N_i \times (C_i - C_{min})]} \times (1 - LP) \quad (3)$$

where C_{avg} is seasonal average $PM_{2.5}$ concentration, N_i denotes the number of trajectories within pathway i, C_i refers to the concentration associated with pathway i, and m represents the total number of pathways. LP (%) indicates the proportion of local concentrations, while P_i represents the regional transport fraction through pathway i.

$$q = 1 - \frac{\sum_{h=1}^{L} N_h \sigma_h^2}{N\sigma^2} \quad (4)$$

where q represents the power of the determinant, N is the total number of samples in the study area, and $h = 1, \ldots, L$ denotes the partitions of factor X; σ^2 and σ_h^2 are the variances of $PM_{2.5}$ concentration Y across the entire region and within partition h, respectively. A higher q value indicates a stronger explanatory power of factor X on $PM_{2.5}$ concentration Y.

2.3.4. Geographical Detector Model (GDM)

The GDM is a newly developed method for analyzing the correlation between $PM_{2.5}$ concentrations and socioeconomic factors [37]. Its core principle is that if an anthropogenic factor exhibits a similar spatial distribution pattern with $PM_{2.5}$ concentrations, it likely contributes to them. A key advantage of the GDM is that it does not rely on a linear assumption when analyzing the anthropogenic factors of spatial stratification heterogeneity, eliminating the need to account for multicollinearity between factors. The influence of driving factors on $PM_{2.5}$ concentration is quantified by the q value [38], calculated as follows:

2.3.5. Potential Source Contribution Function (PSCF) and Concentration–Weighted Trajectory (CWT) Method

The PSCF, a hybrid receptor model [39] based on the backward trajectory, was used to identify the probable potential $PM_{2.5}$ concentration source regions in the CCUA. A higher PSCF value indicates a greater likelihood that the region is a potential source area of $PM_{2.5}$ pollutants [40]. Before conducting the PSCF analysis, the study area for the backward trajectories was divided into 1° resolution grids. Daily average $PM_{2.5}$ concentration exceeding 75 $\mu g/m^3$ was used as the criterion for high $PM_{2.5}$ pollution, in accordance with China's ambient air quality standards (CAAQSs). However, the PSCF method might not differentiate between moderate and strong sources of $PM_{2.5}$. The CWT method was further applied to determine the relative contribution of $PM_{2.5}$ potential sources in the CCUA [41]. To address the uncertainty of fewer $PM_{2.5}$ trajectories in a certain grid, the weighting factor should be multiplied with the PSCF value (WPSCF) and CWT value (WCWT) to reduce its uncertainty [42]. More details of the PSCF and CWT method are available in Zhang et al. [43].

3. Results and Discussion

3.1. Accuracy Assessment of the HASM Method

This study employs HASM to generate 120 monthly spatial distribution maps of $PM_{2.5}$ concentration from March 2014 to February 2024. To further compare its interpolation results, HASM's performance was tested against three traditional spatial interpolation

methods: spline, IDW, and Kriging. The comparative analysis of these methods' accuracy is presented in Table 2.

Table 2. Results of validation for spline, IDW, Kriging, and HASM.

Year	Spline		IDW		Kriging		HASM	
	RMSE	R^2	RMSE	R^2	RMSE	R^2	RMSE	R^2
2014	8.57	0.72	7.32	0.73	7.21	0.72	3.12	0.86
2015	9.12	0.77	7.48	0.75	6.77	0.75	3.61	0.87
2016	8.31	0.76	8.22	0.74	6.31	0.79	2.97	0.89
2017	7.56	0.71	6.92	0.72	7.12	0.73	3.43	0.89
2018	8.57	0.72	8.84	0.78	7.81	0.71	3.12	0.87
2019	9.12	0.77	8.23	0.75	8.76	0.77	3.61	0.84
2020	8.31	0.76	8.09	0.70	8.12	0.72	2.97	0.90
2021	7.56	0.71	7.98	0.79	8.36	0.75	3.43	0.85
2022	8.65	0.74	8.67	0.76	7.95	0.74	3.08	0.81
2023	7.72	0.73	8.45	0.73	8.63	0.78	2.99	0.82

Compared to the three traditional interpolation methods, HASM reduces algorithmic error, demonstrating higher accuracy and lower deviation in interpolating $PM_{2.5}$ concentrations from 2014 to 2024, with R^2 values ranging from 0.81 to 0.90 and RMSE values between 2.97 $\mu g/m^3$ and 3.61 $\mu g/m^3$. HASM addresses interpolation errors, multiscale, and nonlinear problems through the development of least squares optimization [44]. It has been successfully applied to air pollutant interpolation [30]. Consequently, HASM was selected as the optimal method for analyzing the seasonal distribution of $PM_{2.5}$ across the CCUA during this period.

To compare the spatial details and characteristics of $PM_{2.5}$ concentration interpolation results across four methods, this study selected one interpolation result for January 2023 from a set of 120–month $PM_{2.5}$ interpolation data during March 2014 to February 2024 as the case example for presentation (Figures 2 and 3). The results indicate that, although the interpolation results from HASM and the three traditional methods display similar overall spatial patterns, they differ significantly in local details. Especially in areas with sparse $PM_{2.5}$ data, methods like Kriging may exhibit suboptimal prediction performance. As illustrated in Figure 2a, there are notable discrepancies in the northern CCUA, where predictions do not align with actual $PM_{2.5}$ concentrations. Figure 2b,c shows that some local details and abrupt changes in $PM_{2.5}$ concentrations are smoothed out, with noticeable outliers observed in the northwest and central regions of the CCUA. In contrast, the $PM_{2.5}$ results generated by the HASM method algorithm (Figure 2d) provide more accurate predictions in areas with sparse or uneven data and display superior spatial detail and accuracy. This improvement is due to the method's effectiveness in handling complex and non–uniform variations in spatial data. The HASM method performed reasonably well in capturing the $PM_{2.5}$ concentration prediction in the scatter plot diagrams (Figure 3), with an RMSE of 3.43 $\mu g/m^3$ and an R^2 of 0.87.

3.2. Spatial and Temporal Distribution of $PM_{2.5}$

As illustrated in Figure 4, the $PM_{2.5}$ time series shows that the seasonal mean concentration of $PM_{2.5}$ in the CCUA exhibited a fluctuating downward trend. Winter experienced the highest $PM_{2.5}$ pollution compared to other seasons, with the concentration reaching up to 83.84 $\mu g/m^3$ in 2014, and the lowest value of 53.35 $\mu g/m^3$ in 2021. On average, high $PM_{2.5}$ concentrations were observed in winter (74.17 $\mu g/m^3$), followed by spring (47.75 $\mu g/m^3$) and autumn (43.76 $\mu g/m^3$), and then the lowest concentrations were found in summer (32.43 $\mu g/m^3$). This result is generally consistent with previous studies [7].

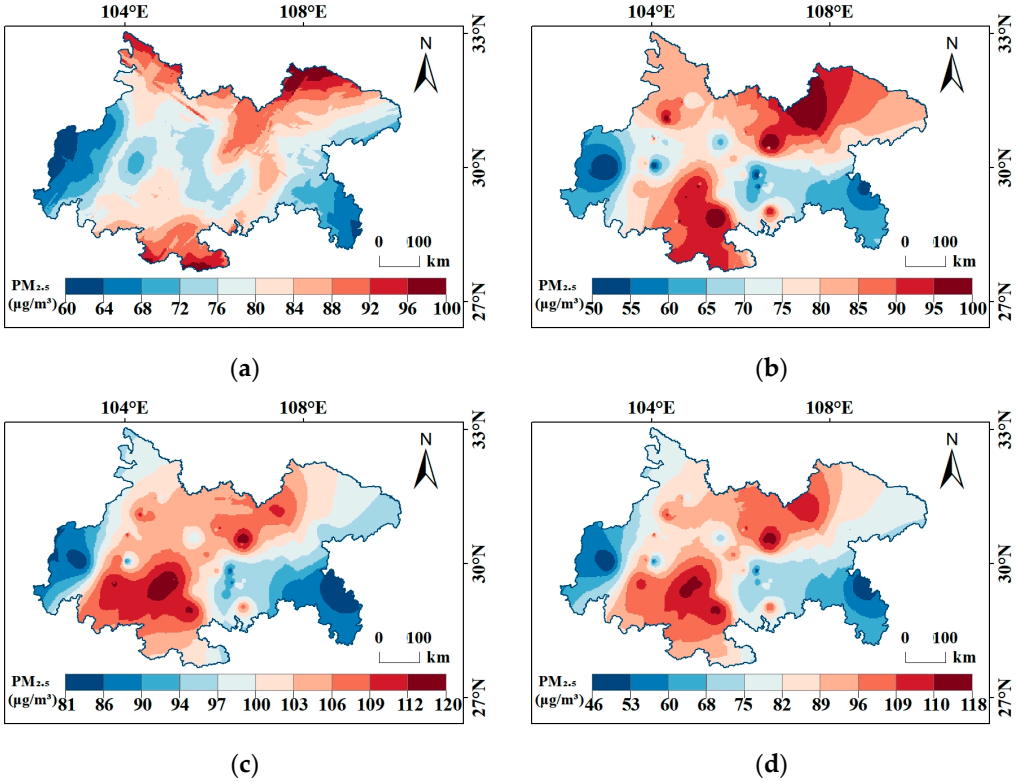


Figure 2. $PM_{2.5}$ concentration interpolation results for the Chengdu–Chongqing Urban Agglomeration in January 2023: (**a**) spline; (**b**) IDW; (**c**) Kriging; (**d**) HASM.

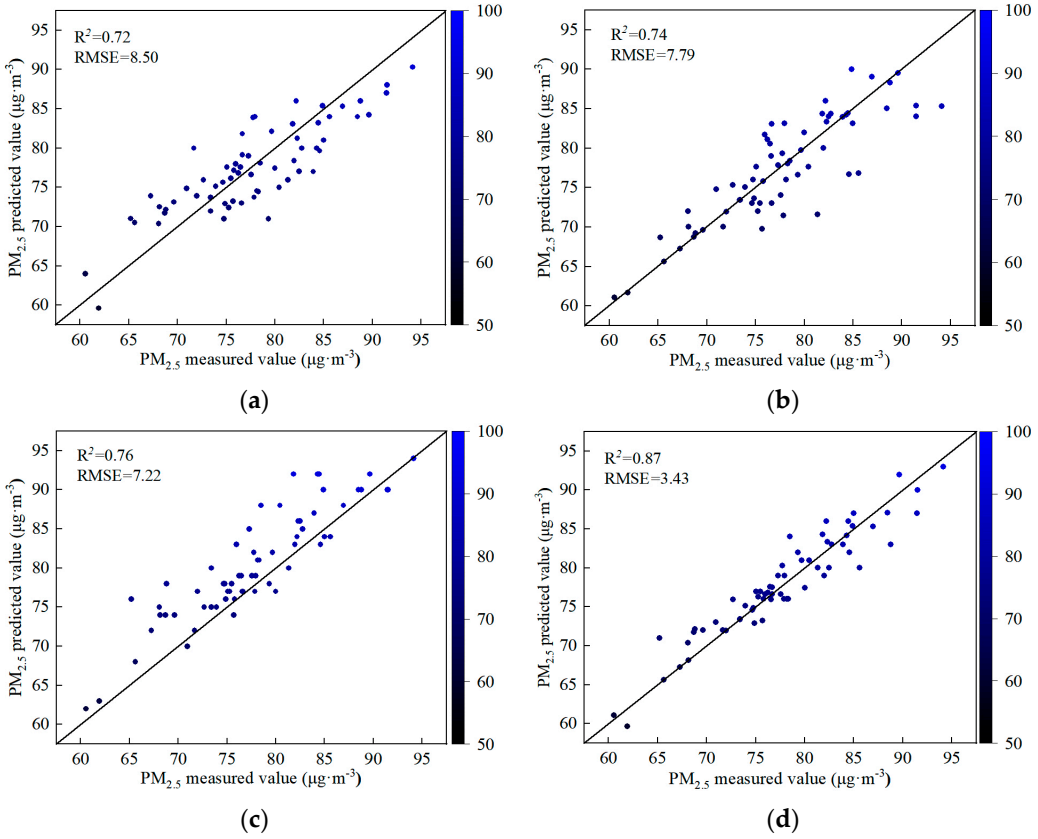


Figure 3. Interpolation accuracy validation of $PM_{2.5}$ concentrations for the Chengdu–Chongqing Urban Agglomeration in January 2023. (**a**) Spline. (**b**) IDW. (**c**) Kriging. (**d**) HASM.

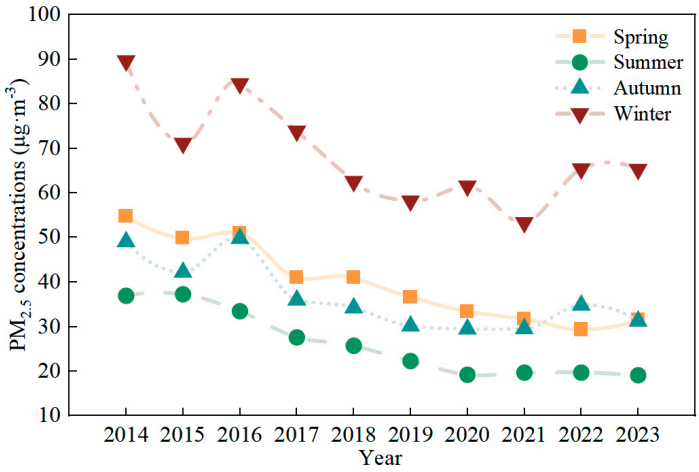


Figure 4. Seasonal variations in $PM_{2.5}$ concentrations in the Chengdu–Chongqing Urban Agglomeration from 2014 to 2023.

Overall, the $PM_{2.5}$ concentration in each season exhibits a distribution pattern with higher values in the southwest and lower in the southeast (Figure 5). Additionally, notable differences are observed in the spatial distribution of $PM_{2.5}$ across different seasons. In winter, $PM_{2.5}$ pollution is most severe, with high concentrations primarily observed in the northeast, northwest, and southwest regions of the CCUA, including cities such as Chengdu, Deyang, and Mianyang; Neijiang, Zigong, and Yibin; and Nanchong, Suining, and Dazhou, respectively. In both spring and autumn, areas with high $PM_{2.5}$ concentrations are predominantly concentrated in the central region of the CCUA, which includes Neijiang city, Ziyang city, and western Chongqing. The southwestern region of the CCUA, which encompasses Zigong city, Yibin city, and Luzhou city. Additionally, the northern region of the CCUA, which includes Nanchong city, Guang'an city, and Dazhou city, also shows high $PM_{2.5}$ concentrations. By summer, pollution drops to its lowest, with no significant high pollution zones evident throughout the study area.

3.3. Evaluating Local and Regional Contributions of $PM_{2.5}$

Twelve clusters and corresponding $PM_{2.5}$ concentrations for each season are based on a total of 148,396 trajectories, and the cluster–mean back trajectories are described in Figures 6 and 7. The speed of air mass movement can be inferred from the length of its trajectory. Longer trajectories indicate faster–moving air masses, while shorter trajectories suggest slower–moving air masses [45]. Table 3 presents the $PM_{2.5}$ concentrations and trajectory proportions for each season from 2014 to 2023. According to the CAAQSs (GB3095–2012) [46], the cluster–mean backward trajectory was classified as polluted (>75 $\mu g/m^3$) and clean (<75 $\mu g/m^3$) pathways. Given the extensive area and complex topography of the CCUA, twelve clusters are evenly distributed between the two centers: the western center of the CCUA (Chengdu) and the eastern center (Chongqing). The average $PM_{2.5}$ concentrations and those exceeding 75 $\mu g/m^3$ were higher in winter compared to the other three seasons.

A cluster–mean back trajectory was defined as a pollution pathway if the proportion of pollution trajectories within that cluster exceeded one–sixth of the total number of pollution trajectories. Among then, the path with the highest percentage of polluted trajectories was defined as the primary pollution pathway for each season.

Seasonal variations of $PM_{2.5}$ concentrations in the CCUA are influenced by both local emissions and regional airmass transport. Local emissions primarily stem from industrial activities, while pollutant transport is largely driven by meteorological conditions. According to the local and regional contribution calculation model in this study, contributions of local and regional area to seasonal $PM_{2.5}$ contribution in the CCUA were obtained, and the results are shown in Table 4.

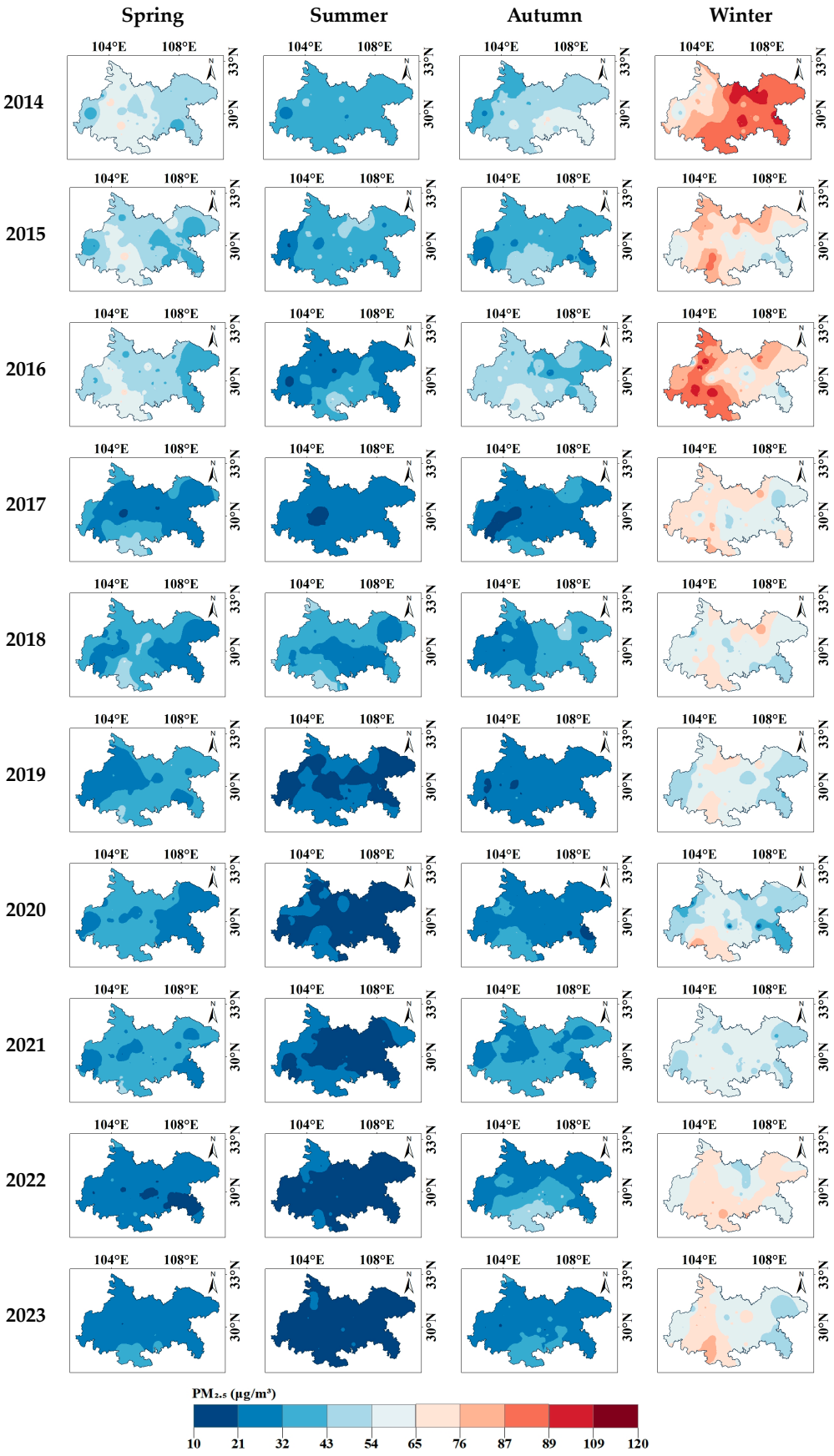


Figure 5. Spatial distribution of seasonal $PM_{2.5}$ concentrations in the Chengdu–Chongqing Urban Agglomeration from 2014 to 2023.

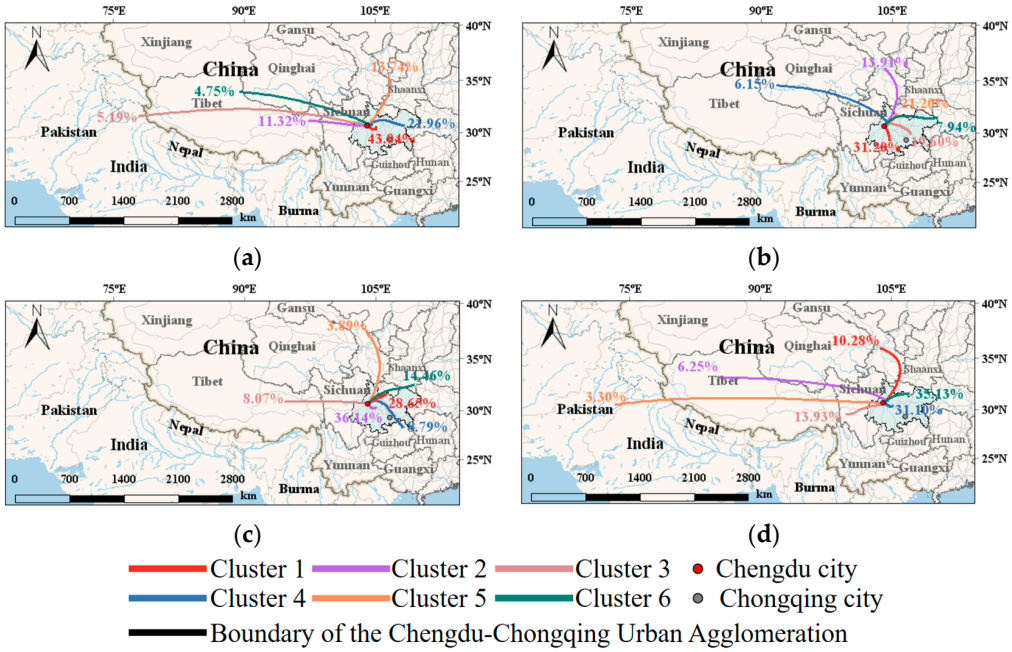


Figure 6. Cluster–mean back trajectories in the western center of the Chengdu–Chongqing Urban Agglomeration from 2014 to 2023 across the four seasons. The percentage indicates the proportion of back trajectories within each cluster relative to the total number of back trajectories. (**a**) Spring. (**b**) Summer. (**c**) Autumn. (**d**) Winter.

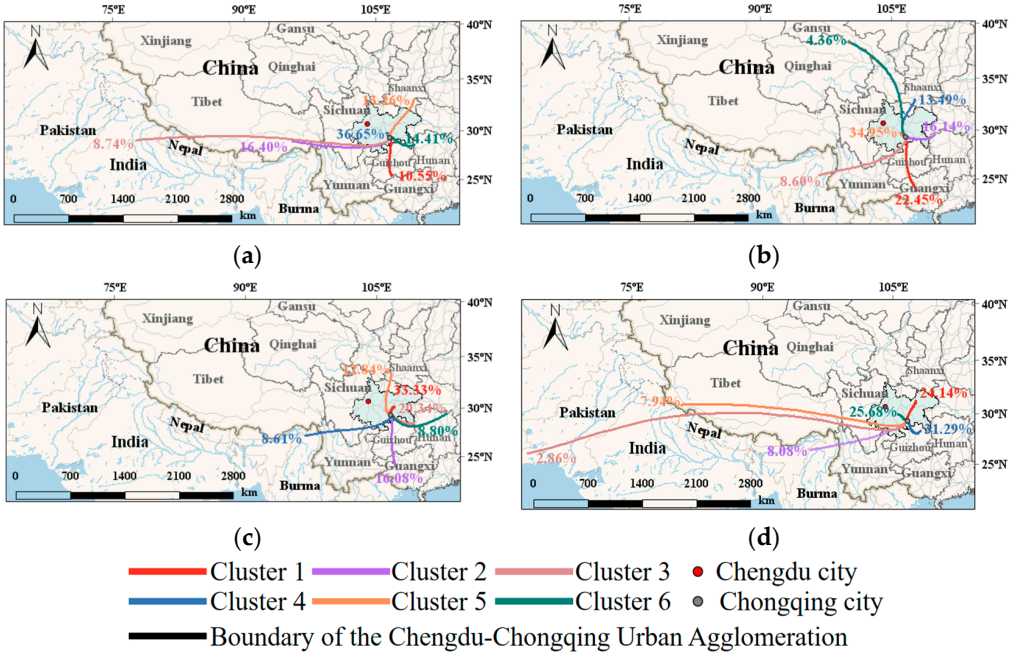


Figure 7. Cluster–mean back trajectories in the eastern center of the Chengdu–Chongqing Urban Agglomeration from 2014 to 2023 across the four seasons. The percentage indicates the proportion of back trajectories within each cluster relative to the total number of back trajectories. (**a**) Spring. (**b**) Summer. (**c**) Autumn. (**d**) Winter.

Table 3. Trajectory percentage and mean $PM_{2.5}$ concentrations in each season from 2014 to 2023.

Season	Cluster	All Trajectories (the Western Center of the CCUA [1]/the Eastern Center of the CCUA)			Polluted Trajectories (the Western Center of the CCUA/the Eastern Center of the CCUA)		
		Percentage (%)	Number	Mean $PM_{2.5}$ Concentrations ($\mu g/m^3$)	Percentage (%)	Number	Mean $PM_{2.5}$ Concentrations ($\mu g/m^3$)
Spring	1	43.04/10.55	8261/1644	65.37/47.30	56.27/12.56	2440/175	110.50/104.27
	2	11.32/16.40	2172/2556	64.88/38.91	11.53/20.62	500/289	108.52/100.16
	3	5.19/8.74	996/1362	33.56/38.17	4.47/7.08	194/100	107.47/103.13
	4	21.96/36.65	4215/5712	66.08/52.72	12.86/28.31	558/400	109.29/105.30
	5	13.74/13.26	2637/2066	46.70/35.71	13.28/18.79	576/265	107.91/98.11
	6	4.75/14.40	911/2246	42.75/42.58	1.59/12.64	68/176	106.26/99.73
Summer	1	31.20/22.45	6371/3858	43.44/34.12	33.80/17.25	583/93	97.91/102.03
	2	13.91/16.14	2840/2774	34.70/26.83	12.52/15.40	216/83	106.75/105.27
	3	19.60/8.60	4002/1478	43.53/34.80	21.97/13.92	379/75	104.95/99.32
	4	6.15/13.49	1255/2318	41.63/28.99	3.25/15.21	56/82	98.87/107.18
	5	21.20/34.96	4329/6006	35.89/29.94	23.94/28.57	413/154	107.91/100.97
	6	7.94/4.36	1621/749	25.21/22.33	4.52/9.65	78/52	107.97/108.02
Autumn	1	28.65/33.33	3571/5530	52.93/38.05	21.07/38.07	980/568	109.77/94.65
	2	36.14/16.08	4504/2667	59.05/34.45	53.98/15.55	2510/232	101.32/98.03
	3	8.07/20.34	1005/3374	42.23/39.41	2.77/17.96	130/268	96.00/90.31
	4	8.79/8.61	1095/1428	36.10/24.95	6.48/3.22	300/48	92.63/91.25
	5	3.89/12.84	485/2130	40.25/48.24	0.86/13.67	40/204	101.00/98.00
	6	14.46/8.80	1802/1460	51.86/30.11	14.84/11.53	690/172	105.35/99.84
Winter	1	10.28/24.14	1769/4805	78.66/73.42	6.82/17.42	486/1092	120.00/108.44
	2	6.25/8.08	1067/1608	97.60/73.42	4.30/4.98	306/312	122.22/108.44
	3	13.93/2.86	2397/569	98.14/63.85	19.46/0.38	1386/24	116.02/128.00
	4	31.10/31.29	5351/6229	75.63/77.93	26.20/53.40	1830/3522	118.06/114.57
	5	3.31/7.95	567/1580	41.96/73.11	2.36/3.92	168/246	141.00/111.39
	6	35.13/25.68	6045/5112	85.71/74.58	40.86/19.90	2910/1248	126.18/117.75

[1] Chengdu–Chongqing Urban Agglomeration.

Table 4. Contributions of local and regional area to $PM_{2.5}$ contribution in the Chengdu–Chongqing Urban Agglomeration from 2014 to 2023 across the four seasons (unit: %).

Area	Spring	Summer	Autumn	Winter
Local areas within the CCUA	26.76	43.15	30.19	15.54
Areas outside of the CCUA	74.24	56.85	69.81	84.46

Across all seasons, the regional contribution to $PM_{2.5}$ in the CCUA region exceeds that of local sources. The highest regional contribution occurs in winter, reaching 84.46%, while the lowest is in summer, at 56.85%, indicating that the primary sources of $PM_{2.5}$ are from areas outside the CCUA on the regional scale and local pollution emission has less impact. As shown in Figure 8, there are no significant seasonal variations in local industrial soot (dust) emissions from 2014 to 2023. ISEs were highest in autumn (1168.37 t), followed by spring (1146.33 t) and winter (1058.15 t), with the lowest in summer (1036.11 t), due to the industrial power restrictions during the summer. This result further demonstrates that regional contributions, rather than local contributions, are the dominant source of seasonal $PM_{2.5}$ in the CCUA.

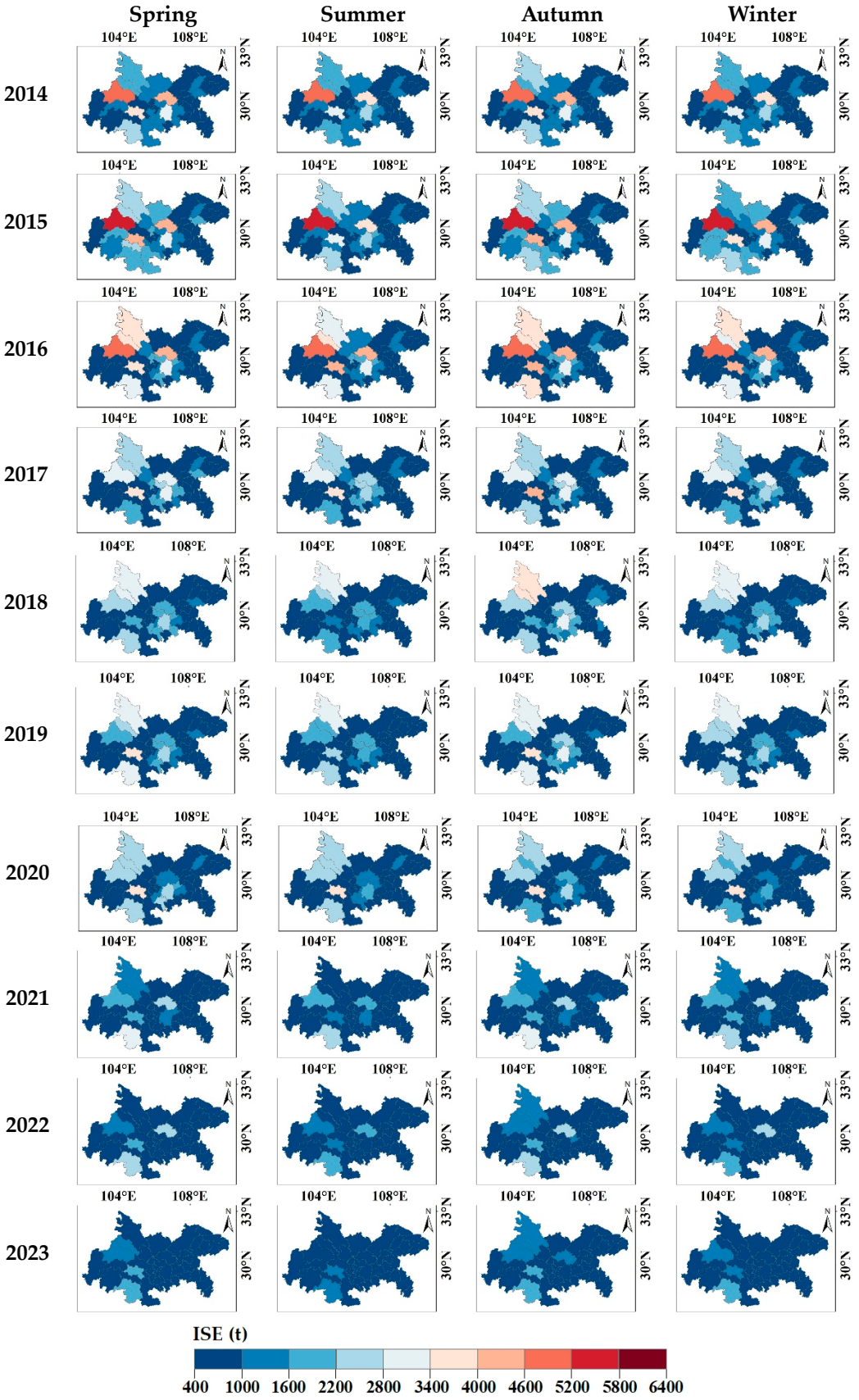


Figure 8. Spatial distribution of seasonal industrial soot (dust) emissions in the Chengdu–Chongqing Urban Agglomeration from 2014 to 2023.

3.4. Relationship Between Seaonal $PM_{2.5}$ Concentration and Its Anthropogenic Factors

The influence (q values) of seven anthropogenic factors on $PM_{2.5}$ concentration were calculated by the GDM (Figure 9). Among these factors, ISE has a dominant influence ($q > 0.4$) on $PM_{2.5}$ concentrations in each season, followed by IS, RD, PD, and GDP. In contrast, EC and FDI showed the least influence. First, the increase in industrial emissions and the proportion of industrial structures lead to higher $PM_{2.5}$ concentrations in each season. This result is because industrial emissions are the primary anthropogenic source of $PM_{2.5}$ concentration in China, producing primary and secondary $PM_{2.5}$ [47,48]. Additionally, the growth of the secondary industry in China is often accompanied by a surge in coal consumption [49], which contributes to higher $PM_{2.5}$ levels. Second, road density reflects the economic level of the CCUA. Higher road density means more vehicle traffic [50], which in turn increases automobile exhaust emissions. This increase is an important factor contributing to the rise in $PM_{2.5}$ concentrations in the CCUA. Third, the increase in population density has been linked to higher anthropogenic emissions, which contribute to $PM_{2.5}$ pollution [51]. In contrast, FDI did not have a significant impact on $PM_{2.5}$ concentrations in any season, likely due to the strict thresholds set for foreign direct investment access in the CCUA.

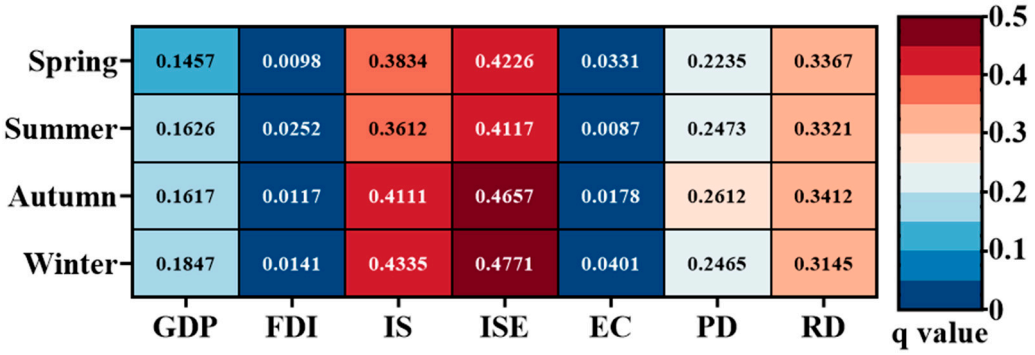


Figure 9. The influence of anthropogenic driving factors in driving seasonal $PM_{2.5}$ concentrations in the Chengdu–Chongqing Urban Agglomeration from 2014 to 2023.

3.5. Backward Trakectory, PSCF, and CWT Analysis

In winter, the pollution pathways in the western center were ranked in descending order as follows: 6 > 4 > 3, while, in the eastern center, the order was 4 > 6 > 1. Among these six major pathways, clusters 6 and 4 accounted for 40.86% and 53.40% of the total polluted trajectories, respectively. Cluster 6 originated from the east (Bazhong City), passed through Nanchong City, and reached Chengdu (Figure 6d). In contrast, cluster 4 started from the south (Tongren City) and traveled southeast through Zunyi City to Chongqing (Figure 7d). This pathway is mostly because clusters 6 and 4 were both short pathways. Suggesting low wind speed, this pathway may exacerbate air pollution. Because of the high population density and the concentration of heavy industries in Nanchong city and Zunyi city, both cities experience significant emissions from vehicle exhaust and industrial production. When air masses pass through these high–emission areas, they are likely to lead to the higher emission of $PM_{2.5}$. Further, weak wind conditions hindered the dispersion of pollutants, causing $PM_{2.5}$ to be carried by the air masses to the CCUA.

In spring and autumn, clusters 1 (Figure 6a) and 2 (Figure 6c), originating from the south (Suining city and Ziyang city, respectively) accounted for the highest percentages of polluted trajectories at 56.27% and 53.98%, respectively, and were identified as the primary pollution pathways in the western center. In contrast, in the eastern center, clusters 4 and 1 had the largest percentages of polluted trajectories, accounting for 28.31% and 38.07%, respectively. Cluster 4 originated from Tongliang District and traveled southeast through Beibei District to Yuzhong District in Chongqing (Figure 7a). Meanwhile, Cluster 1 started in Changshou District and passed through Yubei District before reaching Yuzhong District in Chongqing (Figure 7c). In summer, cluster 1 was the primary pollution pathway in the

western center (Figure 6b), while cluster 5 served as the primary pathway in the eastern center (Figure 7b). The air masses associated with the primary pollution pathways in spring, summer, and autumn all moved slowly and corresponded to short trajectories.

In this study, precipitation, air temperature, relative humidity, and wind speed for each season from 2014 to 2021 were analyzed to assess the effects of meteorological factors on the coverage area of the primary pollution transmission pathways in the CCUA (Figure 10). The results indicate that high precipitation and humidity hinder the dispersion of ground dust and increase the dissolution and erosion of $PM_{2.5}$, resulting in the lowest $PM_{2.5}$ pollution levels during summer. Generally, high wind speeds enhance horizontal diffusion and reduce the accumulation of air pollutants in summer, whereas low wind speed conditions suppress pollutant dispersion, leading to higher $PM_{2.5}$ concentrations in winter. Additionally, elevated summer temperatures promote the development of strong convective weather, facilitating the diffusion of $PM_{2.5}$.

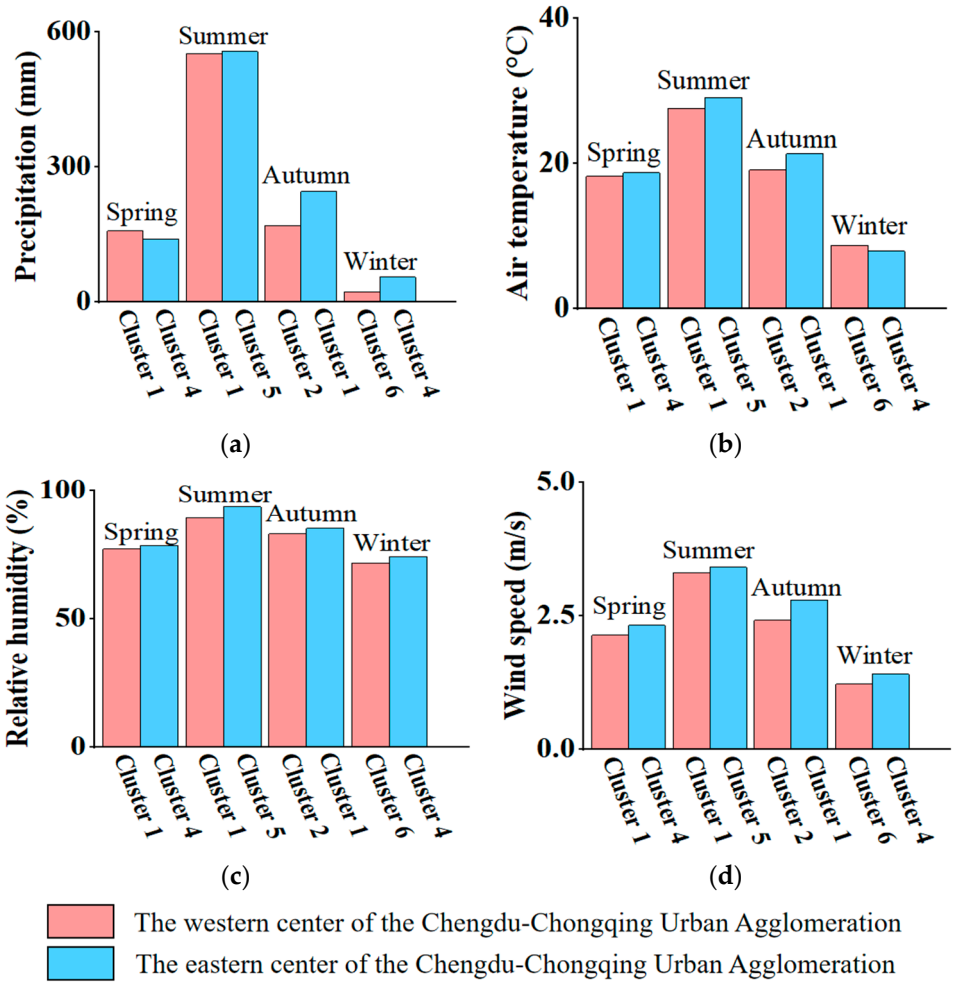


Figure 10. Statistics of four meteorological factors for each season from 2014 to 2021 within the coverage area of the primary pollution pathways for the Chengdu–Chongqing Urban Agglomeration: (**a**) precipitation; (**b**) air temperature; (**c**) relative humidity; (**d**) wind speed.

We identified the probable locations of potential source regions contributing to seasonal $PM_{2.5}$ in the CCUA from 2014 to 2023. The WPSCF map (Figures 11 and 12) distributions varied significantly across seasons due to differences in air masses. In general, the potential source areas in winter were more extensive than those in other seasons, and the main sources were in Xichang city and Nagqu city. In winter, the major source areas of $PM_{2.5}$, with WPSCF values exceeding 0.8, were in the southern Qinghai province, the northern Yunnan province, the border area between the eastern part of the Tibet Au-

tonomous region, and the western Sichuan province (Figures 11d and 12d). The domains of major sources in winter were concentrated in Nagqu city, Xichang city, and Kangding city, which revealed that transport from the west was more important for heavy $PM_{2.5}$ pollution in winter. However, the main potential source areas varied with the seasons. In spring (Figures 11a and 12a), summer (Figures 11b and 12b), and autumn (Figures 11c and 12c), no significant potential source regions were identified, as the WPSCF values were all below 0.8.

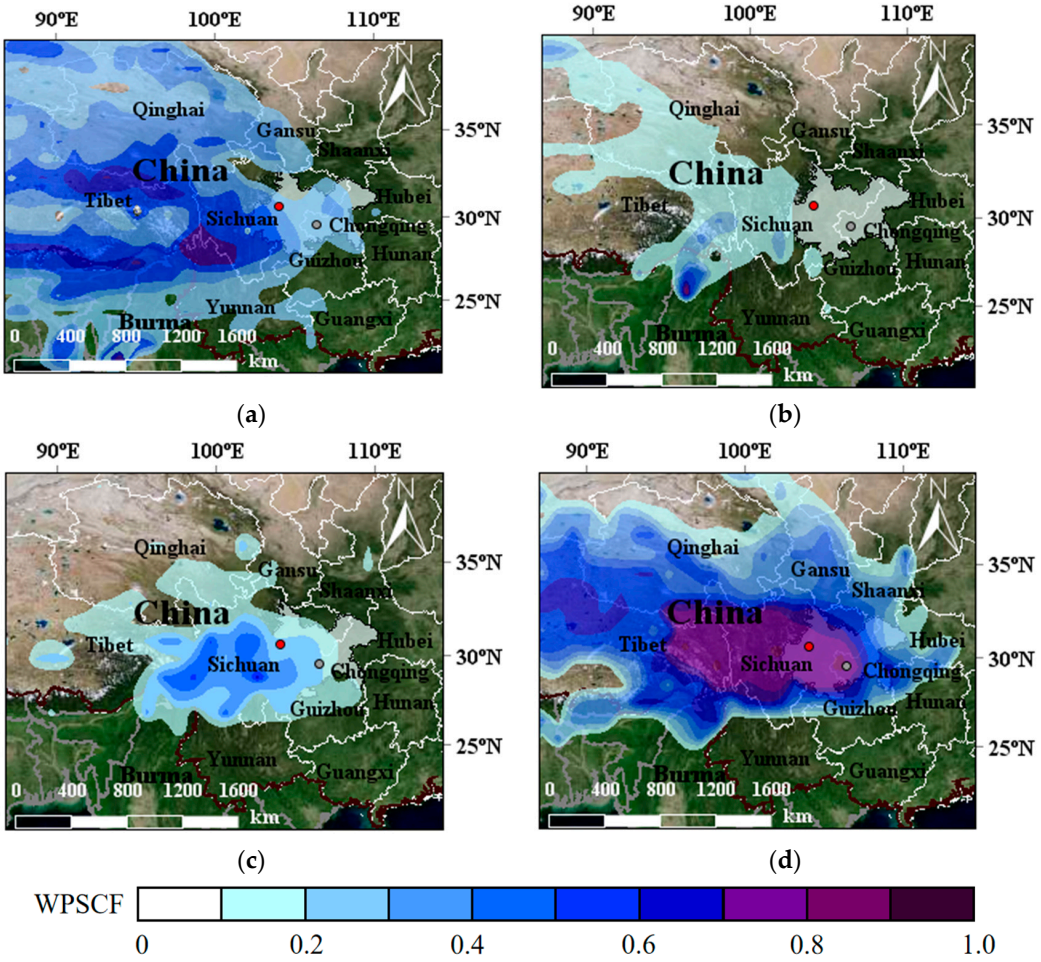


Figure 11. Weighted potential source contribution function (WPSCF) maps for $PM_{2.5}$ in the western center of the Chengdu–Chongqing Urban Agglomeration during 2014–2023 across different seasons. (**a**) Spring. (**b**) Summer. (**c**) Autumn. (**d**) Winter.

The CWT method provides a clearer distinction of pollution levels across different potential source regions, effectively addressing the limitations of the WPSCF. It was employed to assess pollution levels associated with various trajectories, with higher WCWT values indicating greater contributions to $PM_{2.5}$ concentrations in the CCUA. As shown in Figures 13d and 14d, the highest WCWT values during winter are observed at the border area between the eastern part of the Tibet Autonomous Region and western Sichuan province, as well as in the northeastern area of Xichang city and the eastern area of Nagqu city, where $PM_{2.5}$ concentrations reached 85.07 $\mu g/m^3$, 91.25 $\mu g/m^3$, and 80.73 $\mu g/m^3$, respectively. These regions are major contributors to the highest WCWT values, with the northeastern area of Xichang city and the eastern area of Nagqu city even reaching up to 110.00 $\mu g/m^3$. However, during spring (Figures 13a and 14a), summer (Figures 13b and 14b) and autumn (Figures 13c and 14c), no areas in the study region exhibit WCWT values exceeding 100.00 $\mu g/m^3$.

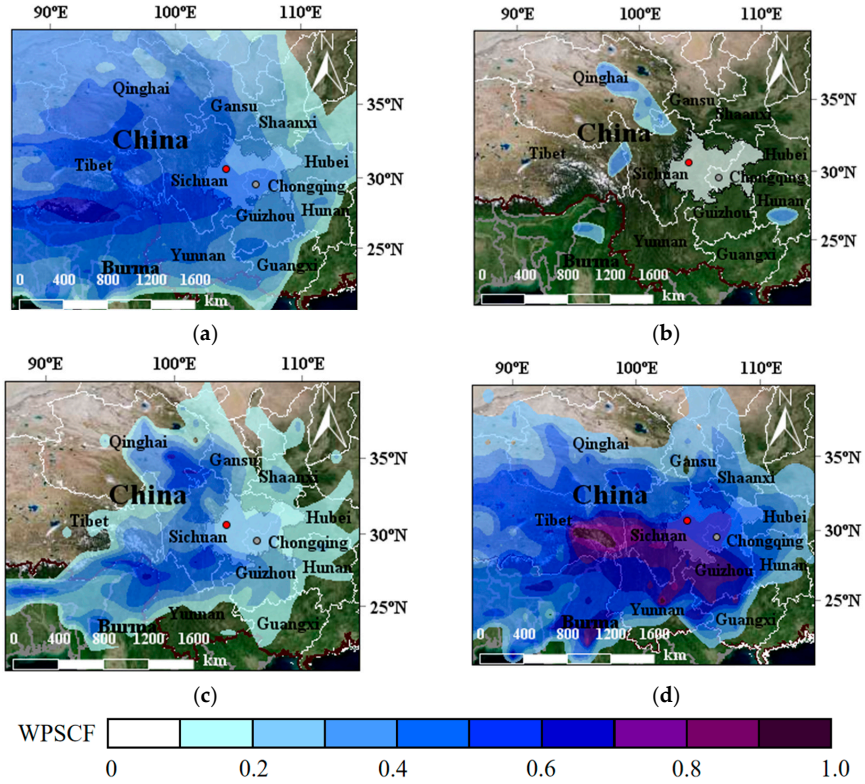


Figure 12. Weighted potential source contribution function (WPSCF) maps for $PM_{2.5}$ in the eastern center of the Chengdu–Chongqing Urban Agglomeration during 2014–2023 across different seasons. (**a**) Spring. (**b**) Summer. (**c**) Autumn. (**d**) Winter.

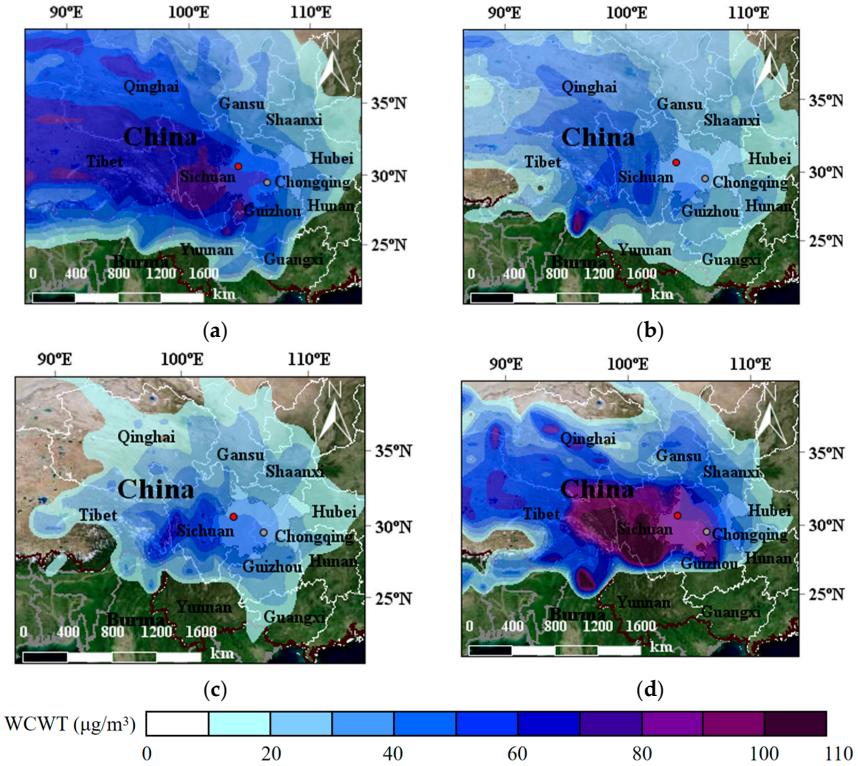


Figure 13. Weighted concentration weighted trajectory (WCWT) maps of $PM_{2.5}$ in the western center of the Chengdu–Chongqing Urban Agglomeration during 2014–2023 across different seasons. (**a**) Spring. (**b**) Summer. (**c**) Autumn. (**d**) Winter.

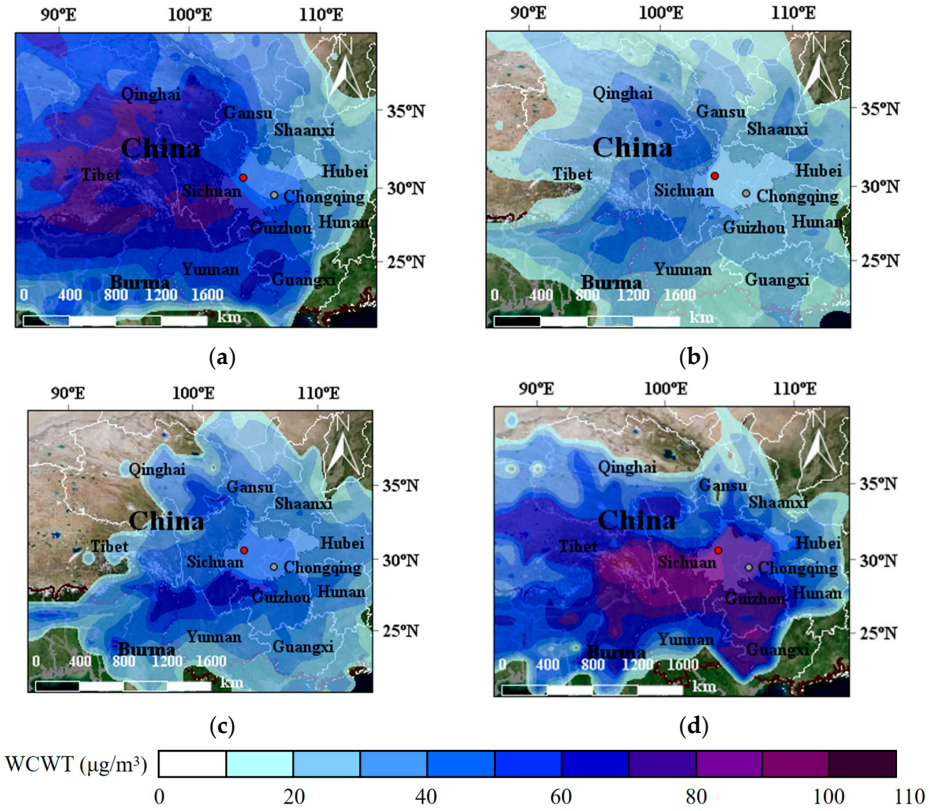


Figure 14. Weighted concentration weighted trajectory (WCWT) maps of $PM_{2.5}$ in the eastern center of the Chengdu–Chongqing Urban Agglomeration during 2014–2023 across different seasons. (**a**) Spring. (**b**) Summer. (**c**) Autumn. (**d**) Winter.

The PSCF and CWT analyses identified similar potential source locations, but the contributions from these locations differed. The major potential source areas identified by the CWT method were generally larger than those determined by the PSCF method, particularly in summer and autumn. This difference suggests that regional sources may have a more significant impact on $PM_{2.5}$ distribution in the CCUA. Notably, significant short–range transport processes contribute to $PM_{2.5}$ levels in the CCUA during winter.

Based on the above considerations, to effectively tackle air pollution issues, the government should focus on a coordinated approach that includes joint prevention and control measures between regions with local and non–local pollution sources. This approach means collaborating with neighboring provinces and cities to reduce the impact of transported pollutants. Additionally, reducing reliance on coal while advancing industrial growth is critical. Greater emphasis should be placed on adopting clean energy alternatives and promoting public transportation to minimize emissions. Furthermore, targeted pollution control strategies should address the specific needs of surrounding regions, such as improving short–distance transport systems and enhancing urban greening efforts, which can help mitigate localized pollution.

4. Conclusions

This study utilized the HASM method to estimate monthly $PM_{2.5}$ concentration in the CCUA. The findings indicate that HASM offers superior accuracy in predicting the spatial distribution of $PM_{2.5}$ compared to traditional interpolation methods. From 2014 to 2023, the seasonal $PM_{2.5}$ concentrations in the CCUA exhibited an overall declining trend. The concentrations varied significantly with the highest levels occurring in winter and the lowest in summer. The ISE and IS are the most important anthropogenic driving factors influencing seasonal $PM_{2.5}$ concentrations. The CCUA is affected by nonlocal $PM_{2.5}$ pollutant transport. According to the regional pollution transport analysis by the PSCF and

CWT method, the border area between the eastern part of the Tibet Autonomous region and the western Sichuan province significantly contributes to $PM_{2.5}$ pollution in the CCUA, especially during winter.

Author Contributions: All authors contributed to the conception and design of this study. K.W.: conceptualization, methodology, formal analysis, data curation, writing—original draft preparation; Y.Y.: conceptualization, software, validation, resources, writing—review and editing; K.M.: methodology, investigation, visualization. All authors have read and agreed to the published version of the manuscript.

Funding: This research was funded by the Natural Science Foundation of Sichuan Province in China (No. 2023NSFSC0752), the National Earth Observation Data Center Foundation in 2021 (No. NODAOP2021009), and the Open Fund of Sichuan Provincial Key Laboratory of Artificial Intelligence (No. 2021RYJ03) support.

Data Availability Statement: All data used in this study are available from the corresponding authors upon reasonable request. The $PM_{2.5}$ monitoring data, socioeconomic data, and meteorological datasets provided by respective agencies and institutions are subject to relevant usage restrictions and permissions.

Acknowledgments: The authors gratefully acknowledge the China National Environmental Monitoring Center for providing the $PM_{2.5}$ monitoring station dataset, as well as the Sichuan Provincial Bureau of Statistics, Chongqing Statistical Bureau, and Sichuan Provincial Department of Transportation for socioeconomic data. We also thank the National Tibetan Plateau Data Center and NOAA for meteorological datasets, all of which were essential to our research and validation efforts. Additionally, we also appreciate the technical guidance from researcher Tianxiang Yue on optimizing the HASM algorithm.

Conflicts of Interest: The authors affirm that there are no personal or financial interests that could have influenced the objectivity of this study.

References

1. Chan, C.K.; Yao, X. Air pollution in mega cities in China. *Atmos. Environ.* **2008**, *42*, 1–42. [CrossRef]
2. Gao, Y.; Shan, H.; Zhang, S.; Sheng, L.; Li, J.; Zhang, J.; Ma, M.; Meng, H.; Luo, K.; Gao, H. Characteristics and sources of $PM_{2.5}$ with focus on two severe pollution events in a coastal city of Qingdao, China. *Chemosphere* **2020**, *247*, 125861. [CrossRef]
3. Liu, L.; Duan, Y.; Li, L.; Xu, L.; Yang, Y.; Cu, X. Spatiotemporal trends of $PM_{2.5}$ concentrations and typical regional pollutant transport during 2015–2018 in China. *Urban Clim.* **2020**, *34*, 100710. [CrossRef]
4. Wang, Y.; Jiang, H.; Zhang, S.; Xu, J.; Lu, X.; Jin, J.; Wang, C. Estimating and source analysis of surface $PM_{2.5}$ concentration in the Beijing–Tianjin–Hebei region based on MODIS data and air trajectories. *Int. J. Remote Sens.* **2016**, *37*, 4799–4817. [CrossRef]
5. Wang, X.; Wei, W.; Cheng, S.; Li, J.; Zhang, H.; Lv, Z. Characteristics and classification of $PM_{2.5}$ pollution episodes in Beijing from 2013 to 2015. *Sci. Total Environ.* **2018**, *612*, 170–179. [CrossRef] [PubMed]
6. Lv, L.; Wei, P.; Hu, J.; Chen, Y.; Shi, Y. Source apportionment and regional transport of $PM_{2.5}$ during haze episodes in Beijing combined with multiple models. *Atmos. Res.* **2022**, *266*, 105957. [CrossRef]
7. Kong, L.; Tan, Q.; Feng, M.; Qu, Y.; An, J.; Liu, X.; Cheng, N.; Deng, Y.; Zhai, R.; Wang, Z. Investigating the characteristics and source analyses of $PM_{2.5}$ seasonal variations in Chengdu, Southwest China. *Chemosphere* **2020**, *243*, 125267. [CrossRef]
8. Liu, X.; Zou, B.; Feng, H.; Liu, N.; Zhang, H. Anthropogenic factors of $PM_{2.5}$ distributions in China's major urban agglomerations: A spatial–temporal analysis. *J. Clean. Prod.* **2020**, *264*, 121709. [CrossRef]
9. Ma, J.; Ding, Y.; Cheng, J.C.; Jiang, F.; Wan, Z. A temporal–spatial interpolation and extrapolation method based on geographic Long Short–Term Memory neural network for $PM_{2.5}$. *J. Clean. Prod.* **2019**, *237*, 117729. [CrossRef]
10. Yang, L.; Xu, H.; Jin, Z. Estimating ground–level $PM_{2.5}$ over a coastal region of China using satellite AOD and a combined model. *J. Clean. Prod.* **2019**, *227*, 472–482.
11. Huang, C.S.; Lin, T.H.; Hung, H.; Kuo, C.P.; Ho, C.C.; Guo, Y.L.; Chen, K.C.; Wu, C.F. Incorporating satellite–derived data with annual and monthly land use regression models for estimating spatial distribution of air pollution. *Environ. Model. Softw.* **2019**, *114*, 181–187. [CrossRef]
12. Deligiorgi, D.; Philippopoulos, K. Spatial interpolation methodologies in urban air pollution modeling: Application for the greater area of metropolitan Athens, Greece. *Adv. Air Pollut.* **2011**, *17*, 341–362.
13. Wong, D.W.; Yuan, L.; Perlin, S.A. Comparison of spatial interpolation methods for the estimation of air quality data. *J. Expo. Sci. Environ. Epidemiol.* **2004**, *14*, 404–415. [CrossRef]
14. Halimi, M.; Farajzadeh, M.; Zarei, Z. Modeling spatial distribution of Tehran air pollutants using geostatistical methods incorporate uncertainty maps. *Pollution* **2016**, *2*, 375–386.

15. Yu, H.; Russell, A.; Mulholland, J.; Odman, T.; Hu, Y.; Chang, H.H.; Kumar, N. Cross–comparison and evaluation of air pollution field estimation methods. *Atmos. Environ.* **2018**, *179*, 49–60. [CrossRef]
16. Sun, W.; Zhu, Y.; Huang, S.; Guo, C. Mapping the mean annual precipitation of China using local interpolation techniques. *Theor. Appl. Climatol.* **2015**, *119*, 171–180. [CrossRef]
17. Fitzner, D.; Sester, M. Estimation of precipitation fields from 1–minute rain gauge time series–comparison of spatial and spatio–temporal interpolation methods. *Int. J. Geogr. Inf. Sci.* **2015**, *29*, 1668–1693. [CrossRef]
18. Aalto, J.; Pirinen, P.; Heikkinen, J.; Venäläinen, A. Spatial interpolation of monthly climate data for Finland: Comparing the performance of kriging and generalized additive models. *Theor. Appl. Climatol.* **2013**, *112*, 99–111. [CrossRef]
19. Goovaerts, P. Kriging and Semivariogram Deconvolution in the Presence of Irregular Geographical Units. *Math. Geosci.* **2008**, *40*, 101–128. [CrossRef]
20. Magnussen, S.; Næsset, E.; Wulder, M. Efficient multiresolution spatial predictions for large data arrays. *Remote Sens. Environ.* **2007**, *109*, 451–463. [CrossRef]
21. Wang, J.; Zhao, M.W.; Jiang, L.; Yang, C.C.; Huang, X.L.; Xu, Y.; Lu, J. A new strategy combined HASM and classical interpolation methods for DEM construction in areas without sufficient terrain data. *J. Mt. Sci.* **2021**, *18*, 2761–2775. [CrossRef]
22. Yue, T.X.; Du, Z.P.; Song, D.J.; Gong, Y. A new method of surface modeling and its application to DEM construction. *Geomorphology* **2007**, *91*, 161–172. [CrossRef]
23. Liu, Y.; Yue, T.; Zhang, L.; Zhao, N.; Zhao, M.; Liu, Y. Simulation and analysis of XCO_2 in North China based on high accuracy surface modeling. *Environ. Sci. Pollut. Res.* **2018**, *25*, 27378–27392. [CrossRef]
24. Shi, W.; Yue, T.; Wang, Z. High accuracy surface modeling method combined with auxiliary variables for soil mapping. In Proceedings of the 2017 IEEE International Geoscience and Remote Sensing Symposium (IGARSS), Fort Worth, TX, USA, 23–28 July 2017; pp. 6083–6086.
25. Jiang, L.; Zhao, M.; Yue, T.; Zhao, N.; Wang, C.; Sun, J. A modified HASM algorithm and its application in DEM construction. *Earth Sci. Inform.* **2018**, *11*, 423–431. [CrossRef]
26. Zhao, N.; Jiao, Y. A new HASM–based downscaling method for high–resolution precipitation estimates. *Remote Sens.* **2021**, *13*, 2693. [CrossRef]
27. Wei, S.-W.; Lu, C.-H.; Liu, Q.; Collard, A.; Zhu, T.; Grogan, D.; Li, X.; Wang, J.; Grumbine, R.; Bhattacharjee, P.S. The impact of aerosols on satellite radiance data assimilation using NCEP global data assimilation system. *Atmosphere* **2021**, *12*, 432. [CrossRef]
28. Yue, T.X.; Song, D.J.; Du, Z.P.; Wang, W. High–accuracy surface modelling and its application to DEM generation. *Int. J. Remote Sens.* **2010**, *31*, 2205–2226. [CrossRef]
29. Liu, Y.; Wu, B.; Yue, T. Spatiotemporal analysis of global atmospheric XCO_2 concentrations before and after COVID–19 using HASM data fusion method. *Front. Environ. Sci.* **2023**, *10*, 1079480. [CrossRef]
30. Liu, Y.; Yue, T.; Jiao, Y.; Zhao, N.; Zhao, M. Temperature changes in the Heihe River Basin based on high accuracy surface modelling. *Meteorol. Appl.* **2019**, *26*, 720–732. [CrossRef]
31. Zhao, N.; Yue, T. A modification of HASM for interpolating precipitation in China. *Theor. Appl. Climatol.* **2014**, *116*, 273–285. [CrossRef]
32. Alsamamra, H.; Ruiz-Arias, J.A.; Pozo-Vázquez, D.; Tovar-Pescador, J. A comparative study of ordinary and residual kriging techniques for mapping global solar radiation over southern Spain. *Agric. For. Meteorol.* **2009**, *149*, 1343–1357. [CrossRef]
33. Lichiheb, N.; Ngan, F.; Cohen, M. Improving the atmospheric dispersion forecasts over Washington, DC using UrbanNet observations: A study with HYSPLIT model. *Urban Clim.* **2024**, *55*, 101948. [CrossRef]
34. Wang, Y.; Zhang, S.; Hong, Q.; Song, H.; Yang, L.; Yang, K.; Xu, H.; Yu, F. Characteristics, non–carcinogenic risk assessment and prediction by HYSPLIT of bioaerosol released from Hospital and Municipal Sewage, China. *Ecotoxicol. Environ. Saf.* **2022**, *246*, 114131. [CrossRef] [PubMed]
35. Trošić Lesar, T.; Filipčić, A. Lagrangian particle dispersion (HYSPLIT) model analysis of the sea breeze case with extreme mean daily PM_{10} concentration in Split, Croatia. *Environ. Sci. Pollut. Res.* **2022**, *29*, 73071–73084. [CrossRef]
36. Lv, B.; Liu, Y.; Yu, P.; Zhang, B.; Bai, Y. Characterizations of $PM_{2.5}$ pollution pathways and sources analysis in four large cities in China. *Aerosol Air Qual. Res.* **2015**, *15*, 1836–1843. [CrossRef]
37. Ding, Y.; Zhang, M.; Qian, X.; Li, C.; Chen, S.; Wang, W. Using the geographical detector technique to explore the impact of socioeconomic factors on $PM_{2.5}$ concentrations in China. *J. Clean. Prod.* **2019**, *211*, 1480–1490. [CrossRef]
38. Zhou, C.; Chen, J.; Wang, S. Examining the effects of socioeconomic development on fine particulate matter ($PM_{2.5}$) in China's cities using spatial regression and the geographical detector technique. *Sci. Total Environ.* **2018**, *619*, 436–445. [CrossRef]
39. Ren, B.; Xie, P.; Xu, J.; Li, A.; Tian, X.; Hu, Z.; Huang, Y.; Li, X.; Zhang, Q.; Ren, H.; et al. Use of the PSCF method to analyze the variations of potential sources and transports of NO_2, SO_2, and HCHO observed by MAX–DOAS in Nanjing, China during 2019. *Sci. Total Environ.* **2021**, *782*, 146865. [CrossRef]
40. Berriban, I.; Azahra, M.; Chham, E.; Ferro-García, M.A.; Milena-Pérez, A.; Nouayti, A.; Orza, J.; Brattich, E.; Tositti, L.; Piñero-García, F. PSCF and CWT methods as a tool to identify potential sources of 7Be and 210Pb aerosols in Granada, Spain. *J. Environ. Radioact.* **2022**, *251*, 106977. [CrossRef]
41. Wang, X.; Chen, L.; Guo, K.; Liu, B. Spatio–temporal trajectory evolution and cause analysis of air pollution in Chengdu, China. *J. Air Waste Manag. Assoc.* **2022**, *72*, 876–894. [CrossRef]

42. Hong, Q.; Liu, C.; Hu, Q.; Xing, C.; Tan, W.; Liu, H.; Huang, Y.; Zhu, Y.; Zhang, J.; Geng, T. Evolution of the vertical structure of air pollutants during winter heavy pollution episodes: The role of regional transport and potential sources. *Atmos. Res.* **2019**, *228*, 206–222. [CrossRef]
43. Zhang, K.; Zhou, L.; Fu, Q.; Yan, L.; Bian, Q.; Wang, D.; Xiu, G. Vertical distribution of ozone over Shanghai during late spring: A balloon–borne observation. *Atmos. Res.* **2019**, *208*, 48–60. [CrossRef]
44. Marquardt, D.W. An algorithm for least–squares estimation of nonlinear parameters. *J. Soc. Ind. Appl. Math.* **1963**, *11*, 431–441. [CrossRef]
45. Wang, L.; Li, W.; Sun, Y.; Tao, M.; Xin, J.; Song, T.; Li, X.; Zhang, N.; Ying, K.; Wang, Y. $PM_{2.5}$ characteristics and regional transport contribution in five cities in southern North China Plain, during 2013–2015. *Atmosphere* **2018**, *9*, 157. [CrossRef]
46. *GB3095-2012*; Chinese Ambient Air Quality Standards. China Environment Publishing Group: Beijing, China, 2012.
47. Timmermans, R.; Kranenburg, R.; Manders, A.; Hendriks, C.; Segers, A.; Dammers, E.; Zhang, Q.; Wang, L.; Liu, Z.; Zeng, L. Source apportionment of $PM_{2.5}$ across China using LOTOS–EUROS. *Atmos. Environ.* **2017**, *164*, 370–386. [CrossRef]
48. Wang, Y.; Chen, J.; Wang, Q.; Qin, Q.; Ye, J.; Han, Y.; Li, L.; Zhen, W.; Zhi, Q.; Zhang, Y. Increased secondary aerosol contribution and possible processing on polluted winter days in China. *Environ. Int.* **2019**, *127*, 78–84. [CrossRef]
49. Hao, Y.; Liu, Y.-M. The influential factors of urban $PM_{2.5}$ concentrations in China: A spatial econometric analysis. *J. Clean. Prod.* **2016**, *112*, 1443–1453. [CrossRef]
50. Li, Z.; Fung, J.C.; Lau, A.K. High spatiotemporal characterization of on–road $PM_{2.5}$ concentrations in high–density urban areas using mobile monitoring. *Build. Environ.* **2018**, *143*, 196–205. [CrossRef]
51. Lou, C.-R.; Liu, H.-Y.; Li, Y.-F.; Li, Y.-L. Socioeconomic drivers of $PM_{2.5}$ in the accumulation phase of air pollution episodes in the Yangtze River Delta of China. *Int. J. Environ. Res. Public Health* **2016**, *13*, 928. [CrossRef]

Disclaimer/Publisher's Note: The statements, opinions and data contained in all publications are solely those of the individual author(s) and contributor(s) and not of MDPI and/or the editor(s). MDPI and/or the editor(s) disclaim responsibility for any injury to people or property resulting from any ideas, methods, instructions or products referred to in the content.